JACS
JOURNAL OF THE AMERICAN CHEMICAL SOCIETY
Article
pubs.acs.org/JACS

# Superconductivity in the Narrow Gap Semiconductor $RbBi_{11/3}Te_6$

Christos D. Malliakas,[†] Duck Young Chung,[†] Helmut Claus,[†] and Mercouri G. Kanatzidis*[,†,‡]

[†]Materials Science Division, Argonne National Laboratory, Argonne, Illinois 60439, United States
[‡]Department of Chemistry, Northwestern University, Evanston, Illinois 60208, United States

Supporting Information

**ABSTRACT:** Superconductivity was discovered in the layered compound $RbBi_{11/3}Te_6$, featuring Bi vacancies and a narrow band gap of 0.25(2) eV at room temperature. A sharp superconducting transition at ~3.2 K was observed in polycrystalline ingots. The superconducting volume fraction of oriented single crystals is almost 100%, confirming bulk superconductivity. Systematic Se and Sb substitutions in $RbBi_{11/3-y}Sb_ySe_xTe_{6-x}$ revealed a dependence of the superconducting transition on composition that can increase the $T_c$ up to ~10%. The $RbBi_{11/3}Te_6$ system is the first member of the new homologous series $Rb[Bi_{2n+11/3}Te_{3n+6}]$ with infinite $Bi_2Te_3$-like layers. The large degree of chemical tunability of the electronic structure of the homology via doping and/or substitution gives rise to a new family of superconductors.

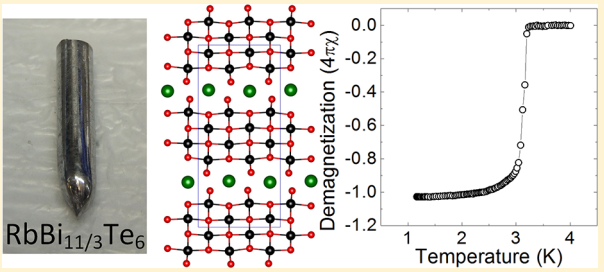


## INTRODUCTION

A layered structure that consists of an alternating stacking of electrically conductive layers separated by insulating layers is an important motif in many unconventional superconductors. Upon proper tuning of the electronic structure via chemical (doping or substitution) or physical pressure, the conducting layers become superconducting, e.g., cuprates[1] and pnictides.[2] The large number of possible configurations of stacking of different types of layered structures and modification of their electronic structure provides a significant opportunity for the discovery of new superconductors. As new families of layered superconductors are discovered, e.g. iron-based superconductors,[3] new insights and information about the mechanism of superconductivity and the possibility of raising the superconducting transition temperature ($T_c$) become available. Superconductivity can also emerge in doped semiconductors. Within the past few years, a new series of Bi chalcogenide-based layered superconductors has emerged composed of layers of $BiQ_2$ (Q = S, Se) coupled with a variety of insulating layers, e.g., $Bi_4O_4(SO_4)Bi_2S_4$ ($T_c \approx 5$ K),[4] $REO_{1-x}F_xBiS_2$, (e.g., RE = La[5] with $T_c \approx 2.5$ K, RE = Ce[6] with $T_c \approx 3$ K, and RE = Nd[7] with $T_c \approx 5.5$ K), $Sr_{1-x}La_xFBiS_2$ ($T_c \approx 3$ K),[8] and $LaO_{0.5}F_{0.5}BiSe_2$ ($T_c \approx 2.6$ K).[9] Additionally, superconductivity in $[Bi_2Te_3]$-like layers separated by $Cs^+$ ions was recently discovered in the narrow gap semiconductor $CsBi_4Te_6$ ($T_c \approx 4.4$ K).[10] Surprisingly, a common feature between the $BiQ_2$ family (i.e., $Bi_4O_4S_3$[11]) and $CsBi_4Te_6$ is the emergence of superconductivity from low-carrier states. Understanding how semiconducting systems with low carrier density can result in superconductivity is a challenge and an opportunity in our search for new superconductors. In this case superconductivity is manifested in systems with intrinsic low carrier density (e.g., ~$10^{19}$ cm$^{-3}$) in contrast to the vast majority of superconductors which have very high carrier densities ($10^{22}$ cm$^{-3}$). Because low carrier density generally leads to a very small density of states (DOS) at the Fermi energy, historically it has not been thought to be conducive to superconductivity. Therefore, such superconducting systems are both interesting and rare.

In this work we report the existence of bulk low-carrier superconductivity at 3.2 K in p-type $RbBi_{11/3}Te_6$,[12] a layered narrow gap $Bi_2Te_3$-based semiconductor which is the first member of the novel homologous series $Rb[Bi_{2n+11/3}Te_{3n+6}]$ and the parent of much larger family $AM_{3+m}Te_{5+m}$ (where A = alkali metal and M = combination of divalent and trivalent metals).

## EXPERIMENTAL SECTION

**Synthesis.** ***Caution!*** *The reaction between Rb and $Bi_2Te_3$ is extremely exothermic. Submilligram quantities of $Bi_2Te_3$ must be used at the initial step of the reaction.*

Stoichiometric $RbBi_{11/3}Te_6$ samples were synthesized by reacting stoichiometric mixtures of Rb, $Bi_2Te_3$, and Te. Substituted samples were synthesized by reacting Rb, $Bi_2Te_3$, Bi, Sb, Se, and Te at the nominal stoichiometry. Starting materials were prereacted in a N2-filled glovebox by adding initially a very small amount of $Bi_2Te_3$ powder in molten Rb metal in fused silica tubes. Once the reaction was completed the rest of the $Bi_2Te_3$ powder (plus Bi, Sb and Se, Te for the substituted samples) was added in the tubes which were evacuated to <$10^{-4}$ mbar and flame-sealed. Tubes were heated to 700 °C at a rate of 1 °C/min in a static rocking furnace, kept at 700 °C for 2 h, rocked in order to facilitate the formation of a homogeneous melt, and then water quenched to room temperature. Tubes were opened in the glovebox, and metallic-looking ingots (Figure 1A) were obtained. Yield of the reaction was ~80% and powder X-ray diffraction showed the presence of $Bi_2Te_3$ second phase in the polycrystalline mixtures. Attempts to synthesize $RbBi_{11/3}Te_6$ by slow cooling of the melt

**Received:** August 20, 2016
**Published:** October 16, 2016



DOI: 10.1021/jacs.6b08732
J. Am. Chem. Soc. 2016, 138, 14694−14698

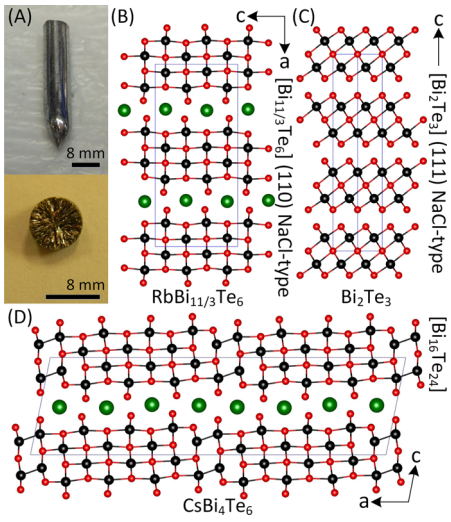


**Figure 1.** (A) As-grown polycrystalline ingot of $RbBi_{11/3}Te_6$ (top) and cross-section of the ingot showing the needle-like morphology of the crystals (bottom) (B) Layered structure of $RbBi_{11/3}Te_6$ viewed down the *b*-axis illustrating similarities and differences with (C) $Bi_2Te_3$ and (D) $CsBi_4Te_6$.

produce larger fractions of $Bi_2Te_3$ second phase. No evidence of glass attack and reaction of the material with the $SiO_2$ walls was observed since Rb was pre-reacted with the starting materials.

Although the superconducting volume fraction is almost 100% measured on isolated bundles of needle-like crystals of $RbBi_{4-x}Te_6$ extracted from the ~10-g-scale ingots, formation of non-superconducting $Bi_2Te_3$ clusters of plate-like crystals dispersed throughout the ingot cannot be avoided. The main reason for the formation of the competing $Bi_2Te_3$ phase is because the melting points of $RbBi_{4-x}Te_6$ (~540 °C) and $Bi_2Te_3$ (~565 °C) are very similar, see differential thermal analysis plot measured at a heating/cooling rate of 5 °C/min, Figure S1. Therefore, any prolonged (>2 h) soaking time of the melt will eventually convert the majority of the material to the most thermodynamically stable $Bi_2Te_3$ phase.

**Electrical Measurements.** We found that the surface of the crystals is very sensitive upon exposure to ambient conditions where the resistivity below $T_c$ does not go all the way down to zero. Mounting of the electrical contacts under inert conditions in an Ar-filled glovebox and protection of the sample with epoxy glue gave zero resistivity values below $T_c$. Resistivity measurements were performed in a quantum design physical property measurement system (PPMS). The standard four-probe technique, employing silver paste contacts cured at room temperature, was used for resistivity measurements, with the electric current applied in an arbitrary direction. Since the surface of the $RbBi_{11/3}Te_6$ system was found to be sensitive upon exposure to ambient conditions, all handling of the materials including mounting of electrical contacts was performed in an Ar-filled glovebox. A small piece was cut from each as-grown polycrystalline ingot, and the specimen was polished to a rectangular shape using sand paper. Bundles of the needle-like crystallites were oriented approximately along the growth direction (*b*-axis) in each specimen. Additionally, samples used for transport measurements were protected by coating them with epoxy glue before taking them outside the glovebox.

The criterion of 50%$\rho_n$ of resistivity was used in order to estimate the upper critical field $H_{c2}(T)$ based on the Ginzburg–Landau (GL) theory using $H_{c2}(T) = H_{c2}(0)(1 - t^2)/(1 + t^2)$, where $t = T/T_c$ is the reduced temperature and $H_{c2}(0)$ is the upper critical field at zero temperature. The Werthamer-Helfand-Hohenberg model was also tested since the spin–orbit coupling is strong in $RbBi_{11/3}Te_6$ using $H_{c2}(0) = -0.693T_c(dH_{c2}/dT)T = T_c$. Room-temperature Hall effect measurements were performed up to 9 T in a PPMS. The magnetic-field dependence of Hall resistivity $\rho_{xy}$ was taken as $\rho_{xy} = [\rho(+H) - (-H)]/2$ at each field point to eliminate the effect of any misalignment of the Hall electrodes.

**Magnetic Measurements.** A home-built low-field quantum interference device (SQUID) magnetometer was used to measure the direct current (dc) magnetization at an applied field of 0.1 mT.[13] Superconducting volume fraction was estimated by converting the magnetic susceptibility data to $4\pi(1 - DF)dM/Hm$, where DF is the demagnetization factor, $d$ the density (g·cm$^{-3}$), $M$ is the magnetic susceptibility (emu), $H$ is the applied field (G), and $m$ the mass of the sample (g). A bundle of $RbBi_{11/3}Te_6$ crystallites oriented parallel to applied magnetic field was used to estimate the superconducting volume fraction. The bundle of oriented crystals was taken from a Travelling Heating Method growth with a hot zone set at 600 °C and cold zone at 350 °C. Sample with approximate dimensions 3.73 ($L$, direction of field) × 0.56 ($W$) × 0.91 ($H$) mm$^3$ and demagnetization factor of 0.0835 were used for the calculation.

The lower critical field $H_{c1}$(T) was measured on a bar-shaped bundle of aligned crystals with dimensions of 3.13 × 2.61 × 4.94 (direction of the field) mm$^3$. For the correction of the sample geometry and calculation of the effective lower critical value ($H_{c1}$*), we used $H_{c1}/H_{c1}^* = \tanh(0.36b/a)^{1/2}$, where $b/a$ is the aspect ratio of the bar-shaped specimen.[14] The GL coherence length $\xi(0)$ is calculated from the upper critical field $H_{c2}(0)$ by $H_{c2}(0) = \Phi_0/(2\pi\xi^2(0))$, where $\Phi_0$ is the magnetic flux quantum and equal to 2.0678 × 10$^{-15}$ T·m$^2$.[15] Similarly, the penetration depth $\lambda(0)$ is given by $\lambda(0) = [\Phi_0/(2\pi H_{c2}(0))]^{1/2}$, which is ~178 nm for $RbBi_{11/3}Te_6$. The corresponding GL parameter $\kappa = \lambda(0)/\xi(0)$ is approximately 7.4.

**Powder X-ray Diffraction.** Ground single crystals of the samples were used to collect powder X-ray diffraction patterns using a PanAlytical X'Pert Pro Powder Diffractometer (Cu K$\alpha$ radiation $\lambda$ = 1.5418 Å) over the 2$\theta$ range of 5–60°, with a step size of 0.02° and a scan speed of 0.25°/min. The measured patterns were compared to the simulated diffraction patterns using the respective single-crystal data. High-resolution powder XRD measurements ($\lambda$ = 0.413894 Å) were performed at beamline BM-11-B at the Advanced Photon Source (APS) at Argonne National Laboratory (ANL). The samples were sealed in Pyrex tubes, placed in Kapton capillaries, and spun at ~600 rpm during collection.

**Density.** Density measurements at room temperature were performed with a Micromeritics AccuPyc 1340 pycnometer based on a gas displacement method. Helium was used as a displacement gas for measuring the volume, which was calculated from the average value of five measurements.

**Vacancies in the $RbBi_{4-x}Te_6$ system.** Single-crystal X-ray crystallography alone did not provide a clear answer about the precise concentration of Bi vacancies in the $RbBi_{4-x}Te_6$ system, Table S1. We have performed a series of refinements against the single-crystal X-ray intensity data by changing the occupancy factor of all Bi sites, Table S2. We tested four different models in which the sum of Bi occupancies in $RbBi_{4-x}Te_6$ was (1) full ($x$ = 0), (2) freely refined, (3) soft constrained to a valence precise value ($x$ = 1/3), and (4) fixed to an arbitrary number ($x$ = 0.5). The SUMP ShelXL command was used in the refinements. The conclusion, after comparing all four agreement factors and crystallographic statistics, is that the refinement is insensitive to changes of the occupancy of the Bi atoms, Table S2. The *R*-value varies between 5.3% for zero vacancies and 5.9% for a massive amount of Bi vacancies ($RbBi_{3.5}Te_6$), indicating that the contrast in the crystallographic agreement factors is not sufficient for drawing any conclusions about the concentration of vacancies in $RbBi_{4-x}Te_6$.

Since the crystallographic analysis in the $RbBi_{4-x}Te_6$ system is not conclusive for giving an accurate determination of the Bi concentration, we utilized density measurements for a better estimation of the amount of vacancies. From Table S2, density appears more sensitive to changes to the $x$-value with values from 7.092 g/cm$^3$ for $x$ = 0 down to 6.655 g/cm$^3$ for $x$ = 0.5.

Density measurements require a relatively large volume of $RbBi_{4-x}Te_6$ sample (~0.5 cm$^3$) in which we had some $Bi_2Te_3$ as a second phase. Therefore, prior to the density measurements, we quantified the amount of $Bi_2Te_3$ impurity in our samples by high-


DOI: 10.1021/jacs.6b08732
J. Am. Chem. Soc. 2016, 138, 14694–14698

resolution X-ray synchrotron radiation. Specimens from four different batches of $RbBi_{4-x}Te_6$ where analyzed by X-ray and density measurements, Table S3. Powder X-ray analyses (Figure S8) gave a molar fraction of 18−20% $Bi_2Te_3$ second phase (one sample measured with synchrotron and all four sample measured with an in-house diffractometer) in the volume of the samples measured in the pycnometer. Average measured density of the samples was 6.99 g/cm$^3$ and taking into account at least 20% of $Bi_2Te_3$ ($d$ = 7.70 g/cm$^3$), the estimated real density of $RbBi_{4-x}Te_6$ (molecular weight of 1618 g/mol) is no more than 6.84(4) g/cm$^3$, which corresponds to an average stoichiometry of $RbBi_{0.31}Te_6$. This indicates that indeed the structure contains a large number of vacancies.

## RESULTS AND DISCUSSION

$RbBi_{11/3}Te_6$ crystallizes in the orthorhombic space group *Pnma* with $a$ = 28.204(9) Å, $b$ = 4.400(1) Å, and $c$ = 12.731(4) Å, and it forms crystals of a needle-like morphology, Figure 1A. $RbBi_{11/3}Te_6$ adopts a layered structure composed of $[BiTe_6]$ octahedral forming defected infinite $[Bi_4Te_6]$ layers which contain one-third of $Bi^{3+}$ vacancies balanced by $Rb^+$ ions sandwiched between the layers, Figure 1B. This gives a valence precise formula ($Rb^+$, 11/3 $Bi^{3+}$, and $6Te^{2-}$) and a semiconducting character.[16] The presence of Bi vacancies in the $RbBi_{11/3}Te_6$ structure was verified by density measurements.

The defected $[Bi_4Te_6]$ layers in the structure of $RbBi_{11/3}Te_6$ can be conceptually derived as (110) excisions of the rock-salt lattice, where the structure of the layers in $Bi_2Te_3$ (Figure 1C) consists of a cut along the (111) plane of the NaCl-type. Although the stoichiometry of orthorhombic $RbBi_{11/3}Te_6$ is similar to the one of monoclinic $CsBi_4Te_6$, their structures and properties are very different since the latter has Bi−Bi bonds in its $[Bi_4Te_6]$ layers that break the infinite layer into $[Bi_{16}Te_{26}]$ ribbon-like fragments, Figure 1D. The common building block in the structures of $Bi_2Te_3$, $RbBi_{11/3}Te_6$, and $CsBi_4Te_6$ is the $[Bi_2Te_3]$ unit that varies in orientation and width; i.e., the direction of the cut of the $[Bi_2Te_3]$ layers is different in $RbBi_{11/3}Te_6$ (from (111) in $Bi_2Te_3$ to (110) in the ternary) and the width is infinite where the $[Bi_2Te_3]$ layers in $CsBi_4Te_6$ are only four units wide, forming $[Bi_{16}Te_{24}]$ blocks interconnected with Bi−Bi bonds. The structural flexibility of the $[Bi_2Q_3]$ block to form layers of different orientation and width is a powerful feature in the design of compounds where their composition and structure can be predicted using the concept of homologous relationships.[17,18]

$RbBi_{11/3}Te_6$ can be synthesized on a multigram scale by direct combination of the starting materials. The product of a typical synthesis in a form of an ingot is shown in Figure 1A. $RbBi_{11/3}Te_6$ has a superconducting transition at 3.2 K at zero field (Figure 2A), and resistivity increases with temperature following a metallic-like or semimetallic behavior.[16] Room-temperature infrared diffuse reflectance spectroscopy indicates the presence of a band gap at 0.25(2) eV.[16] We have performed detailed temperature-dependent resistivity measurements as a function of field and field-dependent magnetic susceptibility measurements as a function of temperature in order to characterize the superconducting properties of $RbBi_{11/3}Te_6$, Figure 2. $T_c$ decreases monotonically with applied field (Figure 2A), and the upper critical field $H_{c2}(T)$ was estimated to be around 0.5 T using either the Ginzburg−Landau (GL) law (0.57(4) T)[19] or the Werthamer-Helfand-Hohenberg (WHH) theory (0.46(4) T)[20] considering the strong spin−orbit coupling, Figure 2B. From the low-field-dependent magnetic susceptibility measurement (Figure 2C) a lower critical field of around 10.4(4) mT was estimated (Figure 2D), which is much

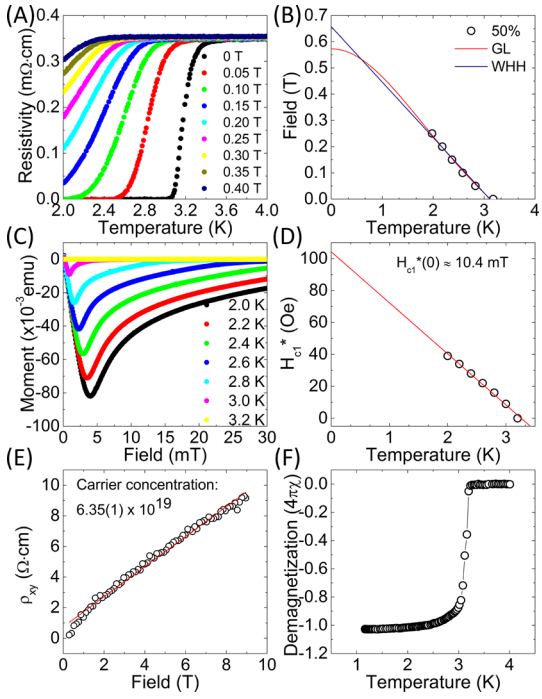


**Figure 2.** (A) Field-dependent resistivity plot of $RbBi_{11/3}Te_6$ showing a sharp superconducting transition at around 3.2 K at zero field. (B) Calculation of upper critical field using the Ginzburg−Landau (GL) theory (red solid line) and the Werthamer−Helfand−Hohenberg (WHH) theory (blue solid line). Both models yield an upper critical field of close to 0.6 T. (C) Field- and temperature-dependent magnetic susceptibility data of $RbBi_{11/3}Te_6$ and (D) Calculation of the lower critical field, which is around 10.4 mT. (E) Field-dependent Hall resistivity measurements of superconducting p-type $RbBi_{11/3}Te_6$ with a carrier concentration of 6.35(1) × 10$^{19}$. (F) Normalized magnetic susceptibility as a function of temperature for oriented single crystals of $RbBi_{11/3}Te_6$ at 0.1 mT. The lower limit of the superconducting volume fraction is almost 100%.

smaller than the value of the upper critical field and consistent with the behavior of a type-II superconductor. From the value of the upper critical field we estimated a GL coherence length $\xi(0)$ of around 24 nm and penetration depth $\lambda(0)$ of around 178 nm,[16] which is comparable to the depth measured in some iron pnictide unconventional superconductors.[21]

The Hall resistivity measurements as a function of field at 5 K of a superconducting sample showed a p-type character with carrier concentration of 6.35(1) × 10$^{19}$ cm$^{-3}$, Figure 2E. This carrier concentration suggests a degenerately doped semiconductor. The samples are hole-doped as they come out of the synthesis. This is typical of bismuth chalcogenides in which anti-site defects and vacancies are common. Such unusually low carrier density for a superconductor was also observed in the $CsBi_4Te_6$ phase,[10] and its correlation to superconductivity is currently unknown. The superconducting volume fraction measured at the plateau below 2 K on a bundle of aligned needle crystals[16] of $RbBi_{11/3}Te_6$ in the zero-field cooled mode was 100% of that expected for full diamagnetism ($1/4\pi$) suggesting that the bulk volume of the sample was superconducting, Figure 2F.

The electronic structure of the layered $RbBi_{11/3}Te_6$ can be modified by a large variety of dopants and/or substitutions performed on each atomic site, as in the chemistry of $Bi_2Te_3$. For example, substitution chemistry between the $[Bi_{11/3}Te_6]$ layers and replacement of the alkali metal ions, and


DOI: 10.1021/jacs.6b08732
J. Am. Chem. Soc. 2016, 138, 14694−14698

substitutions on the Bi and/or the chalcogenide site are possible. Such changes in the electronic structure upon substitution/doping may affect the superconducting transition and ideally increase it to higher temperature. We have performed a series of isovalent substitutions of the $Te^{2-}$ site with $Se^{2-}$ atoms and the $Bi^{3+}$ site with $Sb^{3+}$ atoms and investigated the changes in the superconducting properties of the substituted analogues. We found that there is a superconducting dome in the phase diagram. $T_c$ changes for every substitution made in the series $RbBi_{11/3}Se_xTe_{6-x}$ ($0 < x < 2.1$), $RbBi_{11/3-y}Sb_yTe_6$ (y = 0.3, 0.6), and $RbBi_{11/3-y}Sb_ySe_xTe_{6-x}$ ($x$,$y$ = 0.3), Figure 3. In more detail, every member that contained

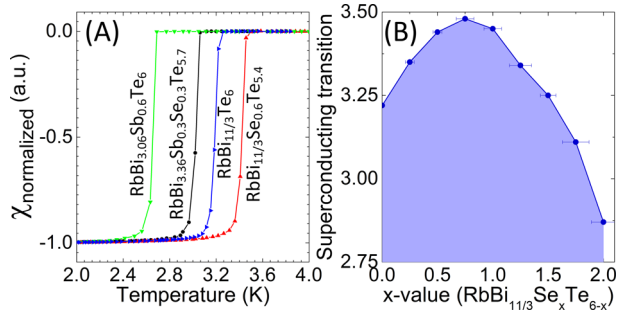


**Figure 3.** (A) Temperature-dependent normalized magnetic susceptibility of Se-substituted $RbBi_{11/3}Se_{0.6}Te_{5.4}$, Sb-substituted $RbBi_3Sb_{0.6}Te_6$, and Se- and Sb-co-substituted $RbBi_3Sb_{0.6}Se_{0.3}Te_{5.7}$ compared against pristine $RbBi_{11/3}Te_6$. Superconducting transition increases with Se substitution up to $x = 0.55(5)$ and decreases for $x > 0.6$ and with any Sb (co)substitution. (B) Phase diagram of superconducting transition as a function of Se concentration ($x$) in $RbBi_{11/3}Se_xTe_{6-x}$ constructed from magnetic susceptibility data and semi-quantitative analyses. Highest $T_c$ was obtained for the optimum Se substitution of $x = 0.55(5)$.

$Sb^{3+}$ showed a lower $T_c$ than the pristine $RbBi_{11/3}Te_6$ (3.2 K) with transitions at 2.6, 2.8, and 3.0 K for $RbBi_{3.06}Sb_{0.6}Te_6$, $RbBi_{3.36}Sb_{0.3}Te_6$, and co-substituted $RbBi_{3.36}Sb_{0.3}Se_{0.3}Te_{5.7}$, respectively, Figure 3A. Interestingly, $T_c$ increases to 3.4 K upon substitution with Se in the $RbBi_{11/3}Se_xTe_{6-x}$ series until an optimum concentration is reached ($x = 0.55(5)$) after which $T_c$ degreases gradually and finally disappears above $x \approx 2.1$ where the solubility limit of Se in $RbBi_{11/3}Te_6$ is reached.[16]

The corresponding phase diagram of the $T_c$ as a function of composition of the $RbBi_{11/3}Se_xTe_{6-x}$ series is shown in Figure 3B which features a dome-like trend which peaks at $x = 0.55(5)$. The change in the electronic structure of the highest $T_c$ $RbBi_{11/3}Se_{0.6}Te_{5.4}$ sample is also reflected in the upper critical field measurement where $H_{c2}(0)$ has increased significantly from 0.5 T (pristine $RbBi_{11/3}Te_6$) to around 1.2 T.[16] The values of upper critical field of the substituted $RbBi_{11/3}Te_6$ members are comparable with those reported for other Bi-containing (e.g., $BiS_2$-based) chalcogenide superconductors.[22]

Unlike the sensitivity of $T_c$ to substitutions in the Bi and Te sublattices, no changes were observed when the stoichiometry of Rb atoms was varied. We performed a series of control experiments by changing the electron count of $Rb_zBi_{11/3}Te_6$ by varying the concentration of Rb ($0.90 \leq z \leq 1.02$ with a step of 0.02). No noticeable change of the $T_c$ was observed[16] in the $Rb_zBi_{11/3}Te_6$ series suggesting that the substitution reactions of Se and/or Sb apply chemical pressure to the $Bi_2Te_3$ layers rather than just occupying vacant sites.

## CONCLUSIONS

The $RbBi_{11/3}Te_6$ and its substitutional variants are rare examples of superconductors in which the emergence of superconductivity is possible through doping of a narrow gap semiconductor. According to Bardeen–Cooper–Schrieffer (BCS) theory electron–phonon coupling and superconductivity can be produced from strong interactions with an ionic component and large electronic density of states (DOS) near the Fermi level. Preliminary band structure calculations suggest the presence of a high DOS composed of Bi and Te bands and located at the top of the valence band just below the Fermi level.[16] We are in the process of mapping the phonon DOS of $RbBi_{11/3}Te_6$ using neutron diffraction in order to study the nature of phonon coupling and probe any similarities or differences with the non-superconducting parent $Bi_2Te_3$. We illustrated that the electronic structure of $RbBi_{11/3}Te_6$ can be modified and $T_c$ can be tuned between 2.6 and 3.6 K with proper isovalent substitution in the $RbBi_{11/3-y}Sb_ySe_xTe_{6-x}$ series. Doping of these narrow gap semiconductors can be also a great potential route for optimizing superconductivity, as shown in $IrTe_2$,[23] $Bi_2Se_3$,[24] and $TiSe_2$.[25]

Structural homologies can be excellent and fertile sources of predictable new materials. They can help us understand relationships among crystal structures, chemical bonding, electronic band structure, and composition across members of a series. The discovery of superconductivity in the $RbBi_{11/3}Te_6$ system forecasts the potential existence of other interesting superconductors in the class $Rb[Bi_{2n+11/3}Te_{3n+6}]$ which is a homology that can be more generally represented as $AM_{3+m}Te_{5+m}$, where A is an alkali metal and M can be a combination of divalent and trivalent metals, e.g., the $CsPb_mBi_3Te_{5+m}$ series.[26]

## ASSOCIATED CONTENT

### Supporting Information

The Supporting Information is available free of charge on the ACS Publications website at DOI: 10.1021/jacs.6b08732.

Energy-dispersive X-ray spectroscopy data, powder X-ray diffraction, additional magnetic susceptibility, field-dependent resistivity data, band gap plots, and DOS, including Figures S1–S10 and Tables S1–S4 (PDF)
Crystallographic information for $RbBi_{11/3}Te_6$ (CIF)

## AUTHOR INFORMATION

### Corresponding Author

*m-kanatzidis@northwestern.edu

### Notes

The authors declare no competing financial interest.

## ACKNOWLEDGMENTS

This work is supported by the U.S. Department of Energy, Office of Science, Basic Energy Sciences, Materials Sciences and Engineering Division. Use of the Advanced Photon Source at Argonne National Laboratory was supported by the U.S. Department of Energy, Office of Science, Office of Basic Energy Sciences, under Contract No. DE-AC02-06CH11357.

## REFERENCES

(1) Bednorz, J. G.; Müller, K. A. *Z. Phys. B: Condens. Matter* **1986**, *64*, 189.
(2) Kamihara, Y.; Hiramatsu, H.; Hirano, M.; Kawamura, R.; Yanagi, H.; Kamiya, T.; Hosono, H. *J. Am. Chem. Soc.* **2006**, *128*, 10012.



DOI: 10.1021/jacs.6b08732
J. Am. Chem. Soc. 2016, 138, 14694–14698

(3) Zhao, J.; Huang, Q.; de la Cruz, C.; Li, S. L.; Lynn, J. W.; Chen, Y.; Green, M. A.; Chen, G. F.; Li, G.; Li, Z.; Luo, J. L.; Wang, N. L.; Dai, P. C. *Nat. Mater.* **2008**, *7*, 953.
(4) Mizuguchi, Y.; Fujihisa, H.; Gotoh, Y.; Suzuki, K.; Usui, H.; Kuroki, K.; Demura, S.; Takano, Y.; Izawa, H.; Miura, O. *Phys. Rev. B: Condens. Matter Mater. Phys.* **2012**, *86*, 220510.
(5) Mizuguchi, Y.; Demura, S.; Deguchi, K.; Takano, Y.; Fujihisa, H.; Gotoh, Y.; Izawa, H.; Miura, O. *J. Phys. Soc. Jpn.* **2012**, *81*, 114725.
(6) Xing, J.; Li, S.; Ding, X.; Yang, H.; Wen, H.-H. *Phys. Rev. B: Condens. Matter Mater. Phys.* **2012**, *86*, 214518.
(7) Demura, S.; Mizuguchi, Y.; Deguchi, K.; Okazaki, H.; Hara, H.; Watanabe, T.; James Denholme, S.; Fujioka, M.; Ozaki, T.; Fujihisa, H.; Gotoh, Y.; Miura, O.; Yamaguchi, T.; Takeya, H.; Takano, Y. *J. Phys. Soc. Jpn.* **2013**, *82*, 033708.
(8) Lin, X.; Ni, X.; Chen, B.; Xu, X.; Yang, X.; Dai, J.; Li, Y.; Yang, X.; Luo, Y.; Tao, Q.; Cao, G.; Xu, Z. *Phys. Rev. B: Condens. Matter Mater. Phys.* **2013**, *87*, 020504.
(9) Krzton-Maziopa, A.; Guguchia, Z.; Pomjakushina, E.; Pomjakushin, V.; Khasanov, R.; Luetkens, H.; Biswas, P. K.; Amato, A.; Keller, H.; Conder, K. *J. Phys.: Condens. Matter* **2014**, *26*, 215702.
(10) Malliakas, C. D.; Chung, D. Y.; Claus, H.; Kanatzidis, M. G. *J. Am. Chem. Soc.* **2013**, *135*, 14540.
(11) Takatsu, H.; Mizuguchi, Y.; Izawa, H.; Miura, O.; Kadowaki, H. *J. Phys. Soc. Jpn.* **2012**, *81*, 125002.
(12) Chung, D.-Y.; Choi, K.-S.; Brazis, P. W.; Kannewurf, C. R.; Kanatzidis, M. G. *MRS Online Proc. Libr.* **1998**, *545*, 65.
(13) Vandervoort, K. G.; Griffith, G.; Claus, H.; Crabtree, G. W. *Rev. Sci. Instrum.* **1991**, *62*, 2271.
(14) Brandt, E. H. *Phys. Rev. B: Condens. Matter Mater. Phys.* **1999**, *60*, 11939.
(15) Tinkham, M. *Introduction to Superconductivity*, 2nd ed.; Dover Books on Physics Vol. i; Dover Publications: Mineola, NY, 2004.
(16) See Supporting Information for more details.
(17) Kanatzidis, M. G. *Acc. Chem. Res.* **2005**, *38*, 359.
(18) Mrotzek, A.; Kanatzidis, M. G. *Acc. Chem. Res.* **2003**, *36*, 111.
(19) Ginzburg, V. L.; Landau, L. D. *Zh. Eksp. Teor. Fiz.* **1950**, *20*, 1064.
(20) Werthamer, N. R.; Helfand, E.; Hohenberg, P. C. *Phys. Rev.* **1966**, *147*, 295.
(21) Charnukha, A.; Post, K. W.; Thirupathaiah, S.; Pröpper, D.; Wurmehl, S.; Roslova, M.; Morozov, I.; Büchner, B.; Yaresko, A. N.; Boris, A. V.; Borisenko, S. V.; Basov, D. N. *Sci. Rep.* **2016**, *6*, 18620.
(22) Mizuguchi, Y. *J. Phys. Chem. Solids* **2015**, *84*, 34.
(23) Yang, J. J.; Choi, Y. J.; Oh, Y. S.; Hogan, A.; Horibe, Y.; Kim, K.; Min, B. I.; Cheong, S. W. *Phys. Rev. Lett.* **2012**, *108*, 116402.
(24) Hor, Y. S.; Williams, A. J.; Checkelsky, J. G.; Roushan, P.; Seo, J.; Xu, Q.; Zandbergen, H. W.; Yazdani, A.; Ong, N. P.; Cava, R. J. *Phys. Rev. Lett.* **2010**, *104*, 057001.
(25) Morosan, E.; Zandbergen, H. W.; Dennis, B. S.; Bos, J. W. G.; Onose, Y.; Klimczuk, T.; Ramirez, A. P.; Ong, N. P.; Cava, R. J. *Nat. Phys.* **2006**, *2*, 544.
(26) Hsu, K.-F.; Chung, D.-Y.; Lal, S.; Mrotzek, A.; Kyratsi, T.; Hogan, T.; Kanatzidis, M. G. *J. Am. Chem. Soc.* **2002**, *124*, 2410.


DOI: 10.1021/jacs.6b08732
*J. Am. Chem. Soc.* 2016, 138, 14694−14698